10834–10848 *Nucleic Acids Research, 2016, Vol. 44, No. 22* *Published online 28 September 2016*
doi: 10.1093/nar/gkw870

Methylation at position 32 of tRNA catalyzed by TrmJ alters oxidative stress response in *Pseudomonas aeruginosa*

Juthamas Jaroensuk[1,2], Sopapan Atichartpongkul[3], Yok Hian Chionh[2], Yee Hwa Wong[4,†], Chong Wai Liew[5,†], Megan E. McBee[2], Narumon Thongdee[1], Erin G. Prestwich[6], Michael S. DeMott[6], Skorn Mongkolsuk[3,7,8], Peter C. Dedon[2,6,*], Julien Lescar[4,5,9,*] and Mayuree Fuangthong[1,3,8,*]

[1]Applied Biological Sciences Program, Chulabhorn Graduate Institute, Bangkok, Thailand, [2]Singapore-MIT Alliance for Research and Technology, Singapore, [3]Laboratory of Biotechnology, Chulabhorn Research Institute, Bangkok, Thailand, [4]School of Biological Sciences, Nanyang Technological University, Singapore, [5]NTU Institute of Structural Biology, Nanyang Technological University, Singapore, [6]Department of Biological Engineering, Massachusetts Institute of Technology, Cambridge, MA, USA, [7]Department of Biotechnology, Faculty of Sciences, Mahidol University, Bangkok, Thailand, [8]Center of Excellence on Environmental Health and Toxicology (EHT), Bangkok, Thailand and [9]UPMC UMRS CR7 - CNRS ERL 8255-INSERM U1135 Centre d' Immunologie et des Maladies Infectieuses, Paris, France

Received August 03, 2016; Revised September 17, 2016; Accepted September 20, 2016

ABSTRACT

Bacteria respond to environmental stresses using a variety of signaling and gene expression pathways, with translational mechanisms being the least well understood. Here, we identified a tRNA methyltransferase in *Pseudomonas aeruginosa* PA14, *trmJ*, which confers resistance to oxidative stress. Analysis of tRNA from a *trmJ* mutant revealed that TrmJ catalyzes formation of Cm, Um, and, unexpectedly, Am. Defined *in vitro* analyses revealed that $tRNA^{Met(CAU)}$ and $tRNA^{Trp(CCA)}$ are substrates for Cm formation, $tRNA^{Gln(UUG)}$, $tRNA^{Pro(UGG)}$, $tRNA^{Pro(CGG)}$ and $tRNA^{His(GUG)}$ for Um, and $tRNA^{Pro(GGG)}$ for Am. $tRNA^{Ser(UGA)}$, previously observed as a TrmJ substrate in *Escherichia coli*, was not modified by PA14 TrmJ. Position 32 was confirmed as the TrmJ target for Am in $tRNA^{Pro(GGG)}$ and Um in $tRNA^{Gln(UUG)}$ by mass spectrometric analysis. Crystal structures of the free catalytic N-terminal domain of TrmJ show a 2-fold symmetrical dimer with an active site located at the interface between the monomers and a flexible basic loop positioned to bind tRNA, with conformational changes upon binding of the SAM-analog sinefungin. The loss of TrmJ rendered PA14 sensitive to H_2O_2 exposure, with reduced expression of *oxyR-recG*, *katB-ankB,* and *katE.* These results reveal that TrmJ is a tRNA:Cm32/Um32/Am32 methyltransferase involved in translational fidelity and the oxidative stress response.

INTRODUCTION

Post-transcriptional ribonucleoside modifications are found in all RNA molecules, with those in tRNA playing roles in tRNA structure and function including maturation, stability, turnover, and fidelity of decoding (1). Modifications on the anticodon stem–loop (ASL) are particularly crucial for maintaining the efficiency and fidelity of translation by stabilizing codon-anticodon pairing, promoting codon recognition, ordering ASL structure, and preventing translational frameshifting (2–5). At the systems level, the dozens of tRNA modifications in yeast have been shown to play critical roles in cellular adaptation to environmental stresses, with reprogramming of tRNA wobble modifications leading to selective translation of critical stress response transcripts (6–8). For example, up-regulation of wobble mcm^5U in $tRNA^{ARG(UCU)}$ by exposure to the DNA-damaging agent, methylmethane sulfonate (MMS), enhanced the translation of transcripts

*To whom correspondence should be addressed. Tel: +66 2 553 8558; Fax: +66 2 553 8572; Email: mayuree@cri.or.th
Correspondence may also be addressed to Julien Lescar. Tel: +65 69 08 22 08; Fax: +65 67 91 38 56; Email: julien@ntu.edu.sg
Correspondence may also be addressed to Peter C. Dedon. Tel: +1 617 253 8017; Fax: +1 617 324 5280; Email: pcdedon@mit.edu
†These authors contributed equally to this work.
Present address: Yok Hian Chionh and Megan E. McBee, Tychan Ltd, Singapore.

enriched with the AGA cognate codon (8), while H_2O_2 exposure increased the level of wobble m^5C in $tRNA^{Leu(CAA)}$, which increased translation of UUG-enriched transcripts that were critical to cellular resistance to H_2O_2 (7). Here, we begin to explore the role of tRNA modifications in the oxidative stress response of prokaryotes, using the PA14 strain of *Pseudomonas aeruginosa.*

As an opportunistic pathogen, *P. aeruginosa* is one of the most common nosocomial pathogens and causes acute and chronic respiratory infections in hospitalized and immunocompromised patients (9), with the US Center for Disease Control and Prevention identifying multidrug-resistant *P. aeruginosa* as a serious threat (10). The complex pathophysiology of *P. aeruginosa* depends on both host response and bacterial virulence factors, with neutrophils playing a particularly important role in *P. aeruginosa* infections (11). As a defense against the reactive oxygen species generated by phagocytes, *P. aeruginosa* possesses a variety of protective mechanisms, including the antioxidant catalases, superoxide dismutases and peroxiredoxins, along with DNA and protein damage repair systems and tight regulation of iron homeostasis (12,13). The *P. aeruginosa* adaptive response to stress is controlled at both transcriptional and post-transcriptional levels, with the well-defined OxyR, SoxR, OhrR and OspR systems regulating transcription of genes having a critical role in pathogenic defense response against oxidative stress (14–17). Conversely, the control of adaptive response to oxidative stress at the post-transcriptional level is poorly understood.

We have identified an *Escherichia coli trmJ* homolog in *P. aeruginosa* (PA14_14690) that confers resistance to oxidative stress. Here, we present a biochemical characterization showing that PA14 *trmJ* encodes a tRNA (cytidine(32)/uridine(32)/adenosine(32)-2′-*O*)-methyltransferase that regulates the expression of oxidative stress response genes. Complementary structural analysis of the catalytic N-terminal domain of TrmJ (TrmJ–NTD) in its free form and bound to the S-adenosyl-L-methionine (SAM) analogue in sinefungin forms a basis to design competitive inhibitors specific for this important human pathogen.

MATERIALS AND METHODS

Chemicals and reagents

Single-stranded synthetic DNAs and PCR primers were purchased from Integrated DNA Technologies. UltraPure™ 1 M Tris–HCl, pH 7.5 and molecular biology grade $MgCl_2$ (1 M) for enzymatic assay were purchased from Thermo, Invitrogen. S-Adenosyl-L-methionine (Adomet or SAM) was purchased from Sigma.

Expression and purification of *P. aeruginosa* PA14 TrmJ

The gene encoding the complete TrmJ (Genbank accession: KFL12361.1) from *Pseudomonas aeruginosa* PA14, with codons optimized for bacterial expression, was purchased from Genscript. The DNA corresponding to the complete TrmJ protein spanning residues 1–257 ('TrmJ') and 1–167 (comprising the N-terminal SAM binding domain, referred to as 'TrmJ–NTD') were cloned into the pNIC28-Bsa4 vector that contains six histidine residues and a TEV cleavage site at the N-terminal end. *E. coli* BL21 (DE3) Rosetta T1R cells were grown at 37°C to an OD_{600} of 1. The proteins were then overexpressed by the addition of 0.5 mM IPTG at 18°C for 18 h. Cells were pelleted and stored at −80°C. All proteins were purified at 4°C. The thawed pellets were resuspended in 30 ml of lysis buffer (20 mM Na-HEPES, pH 7.5, 0.3 M NaCl, 5% glycerol, 0.5 mM TCEP), sonicated in the presence of a cocktail of protease inhibitors (product 539134, Calbiochem), and the lysates were cleared by centrifugation at 22 000 rpm for 30 min. The proteins were purified by immobilized metal affinity chromatography (IMAC) using Ni-NTA agarose (Qiagen) and by size-exclusion on a HiLoad 16/60 Superdex 75 column preparative grade (GE Healthcare) for TrmJ–NTD (20 686 Da, confirmed by mass spectrometry) and on a HiLoad 16/60 Superdex 200 column for TrmJ (31 170 Da). TrmJ was concentrated to 20 mg/ml while TrmJ–NTD was concentrated to 50 mg/ml by ultrafiltration in 20 mM Na-HEPES, pH 7.5, 0.3 M NaCl, 5% (v/v) glycerol, 0.5 mM TCEP. All proteins eluted as dimers in gel filtration.

Bacterial strains, plasmids and growth conditions

The bacterial strains and plasmids used in this study are listed in Supplementary Table S1 (18–23). Bacterial cells were cultured on lysogeny broth with antibiotics at 37°C at the following concentrations: 100 μg/ml amplicillin and 15 μg/ml gentamycin for plasmid maintenance in *E. coli*; 200 μg/ml carbenicillin for plasmid maintenance in PA14 strains; 200 μg/ml carbenicillin, 75 μg/ml gentamycin for maintenance of insertion mutations in *trmJ* mutant strain and $trmJ^C$ strain.

Construction of *trmJ* mutant strain

A *trmJ* mutant strain was constructed by insertional inactivation using a suicide vector pKNOCK-Gm (18). The 200-bp fragment of *trmJ* (PA14_14690) was amplified from the PA14 genomic DNA with primer pairs BT3878/BT3879 (Supplementary Table S2), and cloned into pKNOCK-Gm at *Sma*I site, yielding pKNOCK-*trmJ*. The resulting clone was used to transform *E. coli* BW20767, and *E. coli* BW20767 containing pKNOCK-*trmJ* was used to transfer pKNOCK-*trmJ* into PA14 by conjugation. PA14 transconjugants harboring chromosomal insert of the suicide vectors at *trmJ* gene were selected on lysogeny agar plate containing 75 μg/ml gentamycin and BW20767 was counterselected using 15 μg/ml chloramphenicol. The *trmJ* mutant strain was subsequently screened by colony PCR, and confirmed by Southern blot.

Construction of $trmJ^C$ strain

The primer pairs BT3902/BT3992 (Supplementary Table S2) were used to amplify full length *trmJ* gene (PA14_14690) from the PA14 genomic DNA. Purified PCR product was cloned into pBBR1-MCS4 (21) at *Sma*I site, yielding the complementation plasmid pBBR-*trmJ*. The complementation plasmid was used to transform into *trmJ* mutant strain

by electroporation. The complementation strain is designated *trmJ*^{C}. The *trmJ*^{C} strain was selected on lysogeny agar plate containing 75 μg/ml gentamycin and 200 μg/ml carbenicillin and confirmed by PCR.

Isolation and purification of total tRNA from *P. aeruginosa* strains

Total tRNA was isolated from 50 ml of exponential phase cells ($OD_{600} \approx 0.4$). The cultures were harvested and pelleted by centrifugation at 8000 × g for 10 min at 4°C. The bacterial cell pellet was processed for small RNA species isolation using the PureLink miRNA Isolation Kit following manufacturer's instructions. tRNA in the small RNA population was purified by size-exclusion HPLC using an Agilent SEC3 300 Å, 7.8 × 300 mm column operated at 60°C with a mobile phase of 100 mM ammonium acetate at a flow rate of 0.5 ml/min. tRNA-containing fractions were collected and desalted using an Ambion Millipore 10K MWCO spin-filter system. The quality and concentration of the purified total tRNAs were characterized using a Bioanalyzer (Agilent Small RNA Kit).

In vitro methylation of *P. aeruginosa* TrmJ using total tRNA as a substrate

Total tRNA isolated from PA14 wild-type and *trmJ* mutant strains was used for determining the activity of purified PA14 TrmJ. Five micrograms of total tRNA isolated from PA14 wild-type and *trmJ* mutant were mixed with 50 μM S-adenosyl-L-methionine (SAM) and 5 μM of purified PA14 TrmJ protein in 100 μl reaction volume in 50 mM Tris–HCl, pH 7.5 and 5 mM $MgCl_2$. After incubation at 37°C, the reactions were analyzed as described below (see below).

Identification of tRNA species as substrate for PA14 TrmJ and determination of 2′-*O*-methylation position in tRNA

tRNA substrates for reaction with PA14 TrmJ were prepared by *in vitro* T7 transcription. A series of *P. aeruginosa* tRNA genes were linked to a T7 promoter sequence (Supplementary Table S2) and PCR-amplified using Phusion high fidelity DNA polymerase (Thermo Fisher Scientific) with primers shown in Supplementary Table S2: $tRNA^{Ser(UGA)}$, $tRNA^{Met(CAU)}$, $tRNA^{Trp(CCA)}$, $tRNA^{Gln(UUG)}$, $tRNA^{Pro(GGG)}$ $tRNA^{Pro(UGG)}$, $tRNA^{Pro(CGG)}$ or $tRNA^{His(GUG)}$. PCR product was then used as template for *in vitro* transcription using Megashortscript T7 transcription kit (Ambion) following manufacturer's instructions. At the end of reaction, the DNA template was removed using DNase. The *in vitro* transcribed tRNA was further purified and examined for its quality and concentration as described above. Ten micrograms of *in vitro* transcribed tRNAs were mixed with 50 μM SAM in methylation buffer (50 mM Tris–HCl, pH 7.5 and 5 mM $MgCl_2$) in the presence or absence of PA14 TrmJ. The reactions were incubated at 37°C for 1 h. After incubation, the reactions were collected for analysis by mass spectrometry (see below).

Analysis of ribonucleosides by HPLC-coupled tandem quadrupole mass spectrometry

The ribonucleoside modifications in the various tRNA samples were identified and quantified with chromatography-coupled mass spectrometry (LC–MS) as described previously (24,25). Briefly, tRNA was digested with Benzonase, bacterial alkaline phosphatase, and phosphodiesterase in the presence of deaminase inhibitors (0.5 μg/ml coformycin, 5 μg/ml tetrahydrouridine) and antioxidants (50 μM desferrioxamine, 50 μM butylated hydroxytoluene) at 37°C for 8 h, after which proteins were removed by microfiltration and the filtrate mixtures were analyzed by LC–MS. The ribonucleosides in the enzymatic hydrolysate samples were fractionated on a Thermo Hypersil Gold aQ column (100 × 2.1 mm, 1.9 μm particle size). The mobile phases consisted of 0.1% (v/v) formic acid in water (solvent A) and 0.1% (v/v) formic acid in acetonitrile (solvent B). The samples were fractionated using a flow rate of 0.3 ml/min with a gradient of acetonitrile in 0.1% formic acid as follows: 0–15.3 min, 0%; 15.3–18.7 min, 1%; 18.7–20 min, 6%; 20–24 min, 6%; 24–27.3 min, 100%; and 27.3–41 min, 0%. The HPLC column was maintained at 25°C and directly connected to a triple quadrupole mass spectrometer (Agilent LC/QQQ 6490) operated in positive ion mode. MS parameters were as follows: gas temperature, 50°C; gas flow, 11 l/min; nebulizer, 20 psi; sheath gas flow, 12 l/min; and capillary voltage, 1800 V. The mass spectrometer was operated in MRM mode to detect and quantify ribonucleosides based on the parameters of retention time, m/z of the transmitted parent ion, m/z of the monitored product, fragmentor voltages, and collision energy as noted in Supplementary Table S3. The dwell time was 100 ms. The identities of ribonucleosides were confirmed by comparison of retention time, exact mass, and CID fragmentation to synthetic standards.

RNA fragment analysis HPLC-coupled QTOF mass spectrometry

Five micrograms of *in vitro* methylated tRNA transcripts were digested with either 5 U RNase T1 and dephosphorylated with 10 U bacterial alkaline phosphatase in 10 mM ammonium acetate buffer (pH 7.0) at 37°C for 4 h in the presence of deaminase inhibitors and antioxidants noted earlier, followed by purification of RNA fragments by solid-phase extraction using a $ZipTipC_{18}$ (Millipore). The purified RNA fragments were fractionated by HPLC using an Amide-HILIC, TSK-gel Amide-80 column (2.0 mm ID × 150 mm, 3 μm particle sizes) maintained at 50°C and operated at a flow rate of 0.1 ml/min with a gradient of 8 mM ammonium acetate in acetonitrile as follows: 0–2 min, 10%; 2–3 min, 15%; 3–5.5 min, 30%; 5.5-20.5 min, 60%; 20.5–25 min, 70%; 25–35 min, 10%. Eluent from the HPLC column entered a quadrupole time-of-flight mass spectrometer (Agilent 6520) with an electrospray ionization source operated in negative ion mode. MS parameters were as follows: gas temperature, 325°C; drying gas, 8 l/min; nebulizer, 30 psi; fragmentor voltage, 250 V; skimmer voltage, 65 V, and capillary voltage, 3000 V. The mass range was from m/z 100 to 2000. The MS/MS analysis with collision-induced dissociation (CID) was performed to obtain RNA sequence

information from the RNase T1 digestion products. Collision energies were varied from 25 to 40 V and products were scanned from 100 to 2000 *m/z*. The resulting CID mass spectra were analyzed with SOS (26). The fragment sequences were determined based on their a-B, w and y ions.

Hydrogen peroxide susceptibility test

PA14 wild-type, *trmJ* mutant and *trmJ*^{C} strains were grown to exponential phase at 37°C in lysogeny broth to an OD_{600} of 0.4. Cultures were diluted to an OD_{600} of 0.1 in fresh lysogeny broth and treated with either 0, 5, 10, 15 or 20 mM H_2O_2 for 25 min, followed by 10-fold serial dilutions in PBS buffer. The appropriate cell dilutions were subsequently plated on lysogeny agar plates and incubated overnight at 37°C. Following incubation, colonies were counted and percent surviving of treated cultures was determined relative to the viability of cells without H_2O_2 treatment.

Catalase activity assay

PA14 wild-type, *trmJ* mutant and *trmJ*^{C} strains were grown to exponential phase at 37°C in a shaking incubator in lysogeny broth to an OD_{600} of 0.4 and treated with either 0 or 10 mM H_2O_2 for 25 min. Cell lysates were prepared by sonication and crude protein was used for the catalase activity assay. The catalase activity was measured spectrophotometrically using 10 mM H_2O_2 in 50 mM phosphate buffer, pH 7.0, and reported in specific activity, U mg^{-1} protein. One unit (U) of catalase was defined as the activity that decomposes 1.0 μmol H_2O_2 min^{-1} at pH 7.0 at 25°C.

Semi-quantitative real-time PCR analysis of *oxyR, katA, katB, katE, ankB* and *recG* transcripts in response to H_2O_2

PA14 wild-type, *trmJ* mutant and *trmJ*^{C} strains were grown to exponential phase at 37°C in lysogeny broth to an OD_{600} of 0.4. Cultures were treated with either 0 or 10 mM H_2O_2 for 25 min, followed by extraction of total RNA by hot phenol-chloroform method. The RNA samples were treated with DNaseI and the contamination of genomic DNA in RNA samples with DNaseI treatment were checked by PCR analysis of *16S rRNA*. The RNA integrity was examined with RNA gel electrophoresis. The concentrations of purified RNA samples were measured with Thermo Scientific NanoDrop™ 2000. Two micrograms of purified RNA samples (A260/280 of 2) were reverse transcribed with random hexamer primers using RevertAid Reverse Transcriptase (Thermo Fisher Scientific). Template cDNA (1 ng) and 200 nM primers for either *oxyR, katA, katB, katE ankB, recG* or *16S rRNA* (listed in Supplementary Table S2) were used in 20 μL reaction of KAPA SYBR FAST qPCR kit Master Mix (ABI Prism). The reaction mixtures were incubated for 3 min at 95°C followed by 40 cycles of denaturation at 95°C for 3 s, annealing at 57°C (*16S*, *oxyR*, *recG*, *katE* and *ankB*) and 64°C (*katA* and *katB*) for 20 s and extension at 72°C for 45 s. Data were obtained using STEPONE software v2.1 (Applied Biosystems). The level of *16S rRNA* expression was used to normalize target gene expression in the corresponding strain. The relative gene expression was determined using the $2^{-\Delta\Delta C}{}_{T}$ method (27). Expression of a gene was quantified as fold-change relative to the level in the PA14 wild-type strain without H_2O_2 treatment.

Protein crystallization

Crystallization conditions were screened at 20°C with a concentration of TrmJ–NTD protein of 20 mg/ml using the vapor diffusion method and commercial crystallization screens in Intelli 96-3 wells sitting drop plates. Three precipitant: protein ratios (1:1, 1:2 and 2:1) were tested using a Phoenix crystallization robot (Art Robbins Instruments) and drop volumes of 0.3 μl. Optimized crystals of the free TrmJ–NTD dimer (form I) were obtained using the vapor diffusion method in hanging drops and 24-well trays, by mixing a volume of 1 μl of protein with 2 μl of a precipitant solution containing Bis–Tris propane at pH 6.5, 0.2 M ammonium chloride, 25% (w/v) PEG 3,350. These crystals diffracted to 1.70 Å at SLS. A second crystal form of the TrmJ–NTD dimer was obtained by mixing 1 μl of protein with 2 μl of Morpheus screen conditions A5 (Molecular Dimensions) containing 0.03 M $MgCl_2$, 0.03 M $CaCl_2$, 20% (w/v) PEG MME550, 10% (w/v) PEG 20000, 0.1 M MOPS/Na-HEPES at pH 7.5. These crystals (form II) only diffracted to about 7 Å at SLS. Following three hours soaking with 1 mM sinefungin, however, diffraction to 1.8–2.2 Å was obtained at the Taiwan Light Source.

Data collection and structure determination

Prior to data collection, crystals were briefly soaked in their respective precipitating solution supplemented with 20% (v/v) glycerol and rapidly frozen in liquid nitrogen. X-ray diffraction data were collected at the PXIII beamline at SLS (Villigen, Switzerland) for the free TrmJ–NTD crystal (form I). Free TrmJ–NTD crystal (form II) and the complex with sinefungin were collected at Taiwan Light source NSRRC, beamline 13B1.

Diffraction intensities were integrated with XDS (28), scaled, merged and truncated with SCALA/TRUNCATE (29). The structures of TrmJ–NTD was determined by molecular replacement using the CCP4 software (29) with the structure from *E. coli* (PDB code: 4CND) as search probe. The TrmJ protein from *P. aeruginosa* and *E. coli* share 53% overall amino acid sequence identity. The structure of TrmJ–NTD from *P. aeruginosa* was built iteratively at the computer graphics using COOT (30) and refined using Autobuster (31). The geometrical parameters for sinefungin were generated using coordinates 4R8S from the PDB (www.rcsb.org). Buried solvent accessible surface areas upon dimer formation were calculated using the PDBePISA server (www.ebi.ac.uk/pdbe/pisa/) and structure comparison was performed with the DALI server (http://ekhidna.biocenter.helsinki.fi/dali_server/start). The quality of the structures was assessed using the MOLPROBITY server (molprobity.biochem.duke.edu/) and figures were generated using the Pymol software (Schrodinger). Data collection and structure refinement parameters are summarized in Table 1. The atomic coordinates and structure factors are deposited with the Protein Data Bank under

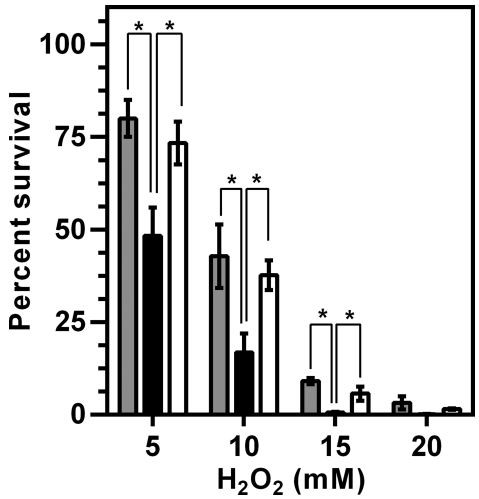

Figure 1. Loss of *trmJ* causes an increased susceptibility to H_2O_2. Phenotypic analysis of cytotoxicity induced by H_2O_2 in PA14 wild-type strain (grey bar), *trmJ* mutant strain (black bar), and the *trmJ* complementation strain or $trmJ^C$ (white bar). The data represent mean ± SD for three biological replicates. Asterisks denote the values with significant difference by Student's t-test ($P \leq 0.05$).

accession codes 5GMC and 5GMB for the free TrmJ–NTD protein, and 5GM8 for TrmJ–NTD bound to sinefungin.

Statistical analysis

Statistical analysis was performed using Graphpad Prism (GraphPad Software). Student's *t*-test was used to determine the statistical significance.

RESULTS

Identification of tRNA-related genes that confer resistance to oxidative stress

Using bioinformatics analysis, we identified 26 genes potentially involved in tRNA modifications in *P. aeruginosa* (Supplementary Table S4). A study in yeast showed that Cm, among other modifications, is increased following exposure to H_2O_2 (6). We then selected PA14_14690 (*trmJ*) whose product is sharing 53% amino-acid sequence identity and 68% similarity to *E. coli* TrmJ and predicted to be involved in the synthesis of Cm for further study. In the H_2O_2 susceptibility assay, we observed that *trmJ* mutant has increased sensitivity to H_2O_2 (Figure 1). That the H_2O_2 sensitivity was due to the loss of *trmJ*, the PA14 mutant lacking this gene was transformed with an expression vector containing full-length *trmJ*, which restored H_2O_2 resistance to wild-type levels (Figure 1).

PA14_14690 encodes a tRNA (cytidine(32)/uridine(32)-2′-*O*)-methyltransferase-like protein of *P. aeruginosa* PA14: PA14 TrmJ

A protein sequence alignment of PA14_14690 with TrmJ homologs with known structure from *E. coli* was constructed using Endscript-http://endscript.ibcp.fr (Figure 2) (32), which revealed that PA14_14690 possesses the conserved region of TrmJ-specific motif, a consensus 'TXARXR' sequence (residues 79–84) (33). This motif has previously been shown to be critical for binding of SAM/SAH and tRNA (33,34). SAM becomes SAH (S−Adenosyl Homocysteine) after losing its methyl group in the methylation reaction. PA14_14690 also contains a conserved arginine at position 23, which is proposed to be involved in its catalytic activity. However, another catalytic residue, the tyrosine at position 141, is replaced by phenylalanine. In addition to arginine positions 82 and 84 in the TrmJ-specific motif, PA14_14690 also contains more key conserved tRNA binding residues including arginine at positions 100, 101 and 105. Therefore, we hypothesized that PA14_14690 encodes a tRNA (cytidine(32)/uridine(32)-2′-*O*)-methyltransferase-like protein. Subsequent biochemical analysis validated this assignment.

Inactivation of *trmJ* abolishes Cm, Um, or Am formation in *P. aeruginosa* tRNA

TrmJ has been reported to methylate the 2′-*O* ribose moiety in tRNA (33,34). Here, we tested this hypothesis for PA14 TrmJ *in vivo* and *in vitro*. Analysis of ribonucleosides in total tRNA from wild-type PA14 by HPLC-coupled triple quadrupole mass spectrometry (LC–MS/MS) relative to standards revealed at least 25 species including Cm, Um and Am (Supplementary Table S3). When we analyzed ribonucleosides in tRNA isolated from the *trmJ* mutant strain, we observed reduced levels of Cm, Um and Am compared to wild-type (Figure 3A). This result suggests that deletion of *trmJ* led to hypo-modification of 2′-*O*-ribose position of C, U and A in tRNA. With respect to the PA14 wild-type strain, the level of Cm, Um and Am was significantly reduced in *trmJ* mutant strain ($P < 0.05$). However, the level of Cm does not drop as much as Um and Am, which suggests functional redundancy for Cm formation.

To further validate formation of Cm, Um, and Am in tRNA by PA14 TrmJ, the sequence encoding the full-length of PA14 TrmJ protein (PA14_14690) was cloned into a plasmid that was used to transform the *trmJ* mutant strain as described in Materials and Methods. LC–MS/MS analysis revealed that restoration of PA14 TrmJ expression in *trmJ* mutant increased the levels of Cm, Um, and Am (Figure 3B) without changing other modifications (Supplementary Table S3). The observation of a higher level of Am in the complemented strain compared to wild-type (Figure 3B) could be due to nonspecific TrmJ activity caused by higher protein levels in the complemented strain, given that complementation was achieved with a medium copy number vector with strong promoter. That TrmJ was responsible for altered levels of Cm, Um and Am was evident in *in vitro* reactions of purified PA14 TrmJ with total tRNA isolated from wild-type and *trmJ* mutant. Significant changes in Cm, Um, and Am levels were only apparent with tRNA isolated from the *trmJ* mutant strain (Figure 4). These results lead to the conclusion that PA14 TrmJ is a 2′-*O*-tRNA methyltransferase catalyzing the formation of Cm, Um and Am.

Table 1. Crystallographic data and refinement statistics for TrmJ–NTD

	TrmJ–NTD-free I	TrmJ–NTD-free II	TrmJ–NTD-sinefungin
Data collection			
X-ray source	SLS X06DA	NSRRC, 13B1	NSRRC, 13B1
Wavelength (Å)	1.000	1.000	1.000
Crystallographic parameters			
Space group	$P2_1$	$P4_32_12$	$P2_1$
Unit cell dimensions (Å)	65.44, 65.04, 93.19	59.80, 59.50, 124.18	56.52, 66.61, 98.58
a, b, c (Å); α, β, γ (°)	90.0, 110.4, 90.0	90.0, 90.0, 90.0	90.0, 101.96, 90.0
Dimers per asymmetric unit	2	0.5	2
Data collection statistic			
Resolution limit (Å)	24.89–1.70 (1.79–1.70)	29.58–1.62 (1.68–1.62)	25.94–2.24 (2.26–2.24)
No. of observed reflections	212 396 (13 543)	288 407 (6001)	123 095 (9971)
No. of unique reflections	75 444 (5209)	29 132 (1200)	34 918 (2849)
Completeness (%)	93.4 (93.4)	95.4 (71.5)	95.5
Redundancy	2.8 (2.6)	9.9 (5.0)	3.5 (3.5)
$I/\sigma(I)$	12.1 (2.5)	19.0 (3.9)	8.0 (1.9)
R_{merge} (%)	0.042 (0.416)	0.062 (0.73)	0.099 (0.635)
Refinement			
Reflections used for refinement	75 444	27 532	34 917
Correlation coefficient	0.954	0.953	0.942
R factor (R_{work}/R_{free}) (%)	17.7/19.9	17.9/20.4	0.19/0.22
Model contents			
Protein atoms	5,155	1,295	5,172
Water molecules	652	166	286
Ligand atoms	–	–	5172
Root mean square deviation			
Distances (Å)	0.010	0.010	0.010
Bond angles (°)	1.01	1.02	1.10
Ramachandran plot			
Favored	92.3	91.2	91.9
Allowed	7.7	9.8	8.1
Outlier	0	0	0
PDB Code	5GMC	5GMB	5GM8

[a] $R_{merge} = \Sigma|I_{obs} - I_{av}|/\Sigma I_{av}$, over all symmetry-related observations.
[b] $R_{work} = \Sigma|F_{obs} - <|F_{calc}|>|/\Sigma|F_{obs}|$, over all reflections included in the refinement.
[c] R_{free} is calculated with 5% of reflections excluded from the refinement. In this formula, $<|F_{calc}|>$ denotes the expectation value of $|F_{calc}|$ under the probability distribution used to define the likelihood function that is maximized in the refinement. Values in parentheses are for the outermost resolution shell of data.

PA14 TrmJ catalyzes 2′-*O*-methylation of C, U and A at position 32 in the tRNA anticodon loop

The preceding results establish that PA14 TrmJ is a 2′-*O*-tRNA methyltransferase but without regard to location. Since *E. coli* TrmJ methylates position 32 in the tRNA anticodon loop, we sought to map the location of PA14 TrmJ products in tRNA. We first identified substrate tRNAs for PA14 TrmJ using the *in vitro* methylation assay with tRNAs synthesized by *in vitro* transcription. As candidate tRNAs, we chose four *P. aeruginosa* tRNA isoacceptors previously reported as substrates for *E. coli* TrmJ: $tRNA^{Ser(UGA)}$ (Cm32) $tRNA^{Met(CAU)}$ (Cm32), $tRNA^{Trp(CCA)}$ (Cm32) and $tRNA^{Gln(UUG)}$ (Um32), as well as four tRNA species possessing A or U at position 32: $tRNA^{Pro(GGG)}$ (Am32), $tRNA^{Pro(UGG)}$ (Um32), $tRNA^{Pro(CGG)}$ (Um32) and $tRNA^{His(GUG)}$ (Um32). The results from LC–MS/MS quantification of Cm, Um and Am in these reactions are shown in Figure 5. All tRNA species except $tRNA^{Ser(UGA)}$ proved to be substrates for PA14 TrmJ, though $tRNA^{His(GUG)}$ was minimally modified. $tRNA^{Pro(GGG)}$ was the most efficient substrate, with Am formation an order of magnitude higher than Um or Cm in the other substrates.

To confirm the location of PA14 TrmJ methylation, $tRNA^{Pro(GGG)}$ and $tRNA^{Gln(UUG)}$ were subjected to *in vitro* methylation by PA14 TrmJ and the modification at position 32 assessed by LC-QTOF mass spectrometric analysis of RNase T1 digests of the tRNAs. As shown in Figure 6A, a doubly-charged negative ion with m/z 617.6017 was detected at 18.9 min in the RNase T1 digestion of $tRNA^{Pro(GGG)}$, which is consistent with CAmUG. This sequence was corroborated in CID analysis (Figure 6B and C). Similarly, a doubly-charged negative ion with m/z 759.5922 was detected at 19.9 min, with subsequent CID analysis consistent with UmUUUG released from $tRNA^{Gln(UUG)}$ (Figure 6D–F). Based on these results, we conclude that PA14 TrmJ catalyzes 2′-*O*-ribose methylation at position 32 in the tRNA anticodon loop.

Structure of the N-terminal domain of TrmJ from *P. aeruginosa*

Initial attempts to crystallize the full-length TrmJ protein from *P. aeruginosa* yielded only poorly diffracting crystals. Sequence comparison with the TrmJ protein from *E. coli* (34) suggested that residues 166-GKPTKMEK-173 connect the N- to the C-terminal domain of TrmJ in a flexible way in the absence of a tRNA ligand. We set out to first

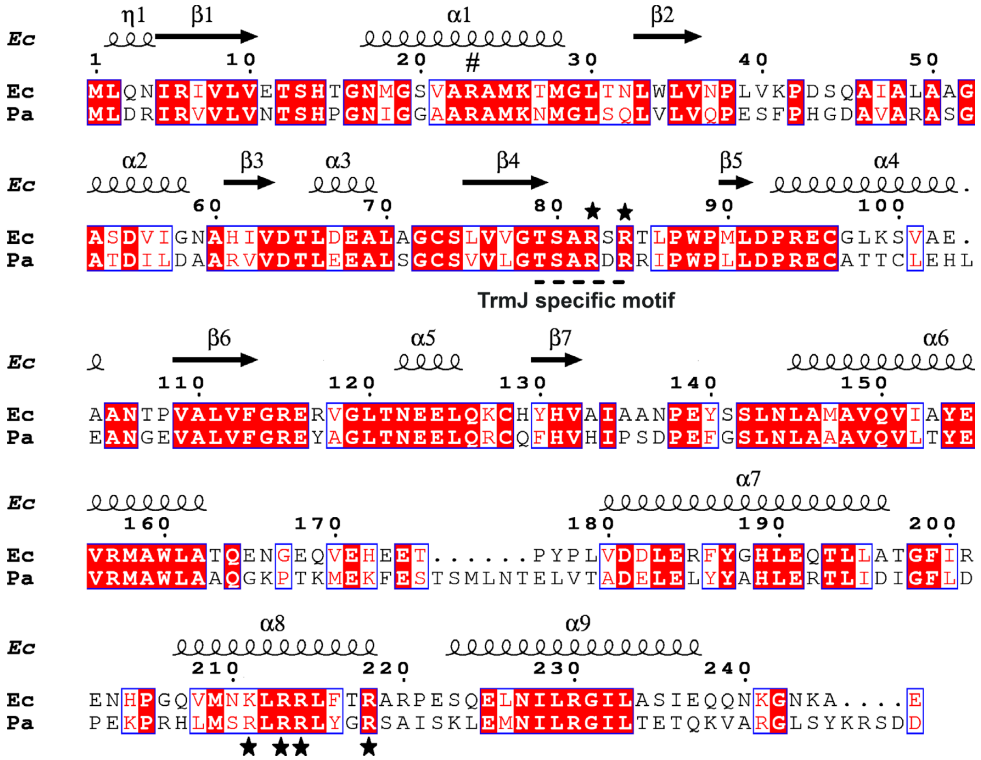

Figure 2. Amino acid sequence alignment of TrmJ proteins. The TrmJ-specific motif is underlined (dashed line) and identical residues are highlighted in red. Residues known to be involved in tRNA binding and catalytic activity of TrmJ (33) are marked by ⋆ and #, respectively. Abbreviations: Ec, *Escherichia coli*; Pa, *Pseudomonas aeruginosa*.

determine the structure of the N-terminal catalytic domain of TrmJ (hereafter named TrmJ–NTD) spanning residues 1 to 167 of the protein by eliminating this source of conformational heterogeneity hindering formation of well-ordered crystals. The TrmJ–NTD protein was obtained with a good yield and crystallized readily in two forms using two distinct sets of precipitants (labeled as 'free I' and 'free II' Table 1). A summary of diffraction data collection and structure refinement statistics for TrmJ–NTD is given in Table 1. The TrmJ–NTD monomer adopts the 'SPOUT' fold (35) – a variant of the classical Rossmann nucleotide-binding fold with the N- and C-termini in close proximity and a central β-sheet composed of seven parallel β-strands surrounded by eight α-helices (Figure 7A and B). The additional four residues derived from cloning at the N-terminal end of the polypeptide participate in the formation of helix α1. A peculiar topological feature also found in other SPOUT methyltransferases is the presence of a knot in the C-terminal region of the protein (Figure 7B). An automatic superimposition of TrmJ–NTD from *P. aeruginosa* with structures deposited in the PDB returned TrmJ from *E. coli* (residues 1–164, PDB code: 4CND) as the closest homologue (59% amino-acid sequence identity) with r.m.s.d. of 1.3 Å (34). Both proteins are tRNA cytidine/uridine 2′-*O*-methyltransferase. The TrmJ–NTD structure is also closely related to various putative ribosomal RNA methyltransferases including HI038 from *Haemophilus influenzae* (PDB code: 3ILK), SpoU from *Rhodobacter sphaeroides* (PDB code: 3ONP) and the RlmB 23S rRNA methylransferase from *E. coli* (PDB code: 1GZ0, (36)) that founded this family of methyltransferases (36). A structure-based sequence alignment is displayed in Figure 7. Both the free and sinefungin bound TrmJ–NTD crystals contain two dimers per asymmetric unit consistent with the observation that the protein eluted as a dimer in gel filtration. The buried surface area at the interface of the TrmJ–NTD dimer is 1210 Å^2, which represents approximately 14% of the total accessible surface area per monomer (8430 Å^2) and is comparable to the interface between the N-Terminal Domain (NTD) of TrmJ from *E. coli* of 1400 Å^2 (34), reflecting the conserved mode of TrmJ dimerization between the two species. Dimerization of the NTD is mediated mainly by the centrally located helix α8 that crisscrosses with its counterpart from the adjacent monomer as well as by one face of β-turn 136–142 that interacts with α2 from the other monomer, while it also forms part of the cofactor binding pocket, on its opposite face (Figures 7 and 8).

Structure of TrmJ–NTD bound to sinefungin and tRNA binding

A crystal form with two TrmJ–NTD dimers per asymmetric unit, was obtained in the presence of PEG MME550 and PEG 20000, but these crystals diffracted very poorly in the absence of bound ligand. Nevertheless, these crystals could be used to obtain a complex between TrmJ–NTD and the isosteric SAM analogue sinefungin by soaking for 3 h leading to good diffraction (Table 1), while soaking of free I native crystals led to severe degradation of their diffraction quality. Each TrmJ–NTD dimer binds two sinefun-

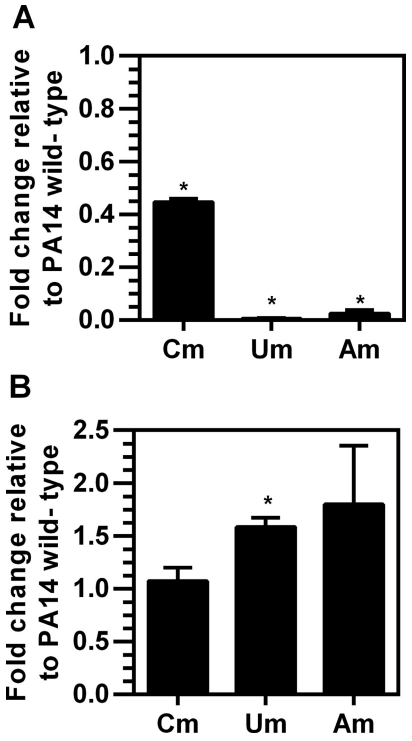

Figure 3. Loss of TrmJ reduces levels of Cm, Um and Am in total tRNA. The levels of Cm, Um and Am in tRNA isolated from wild-type, *trmJ* mutant and *trmJ*^{C} strains of PA14 were quantified by LC–MS/MS. Relative to wild-type cells, loss of TrmJ in *trmJ* mutant strain lowered levels of Cm, Um and Am (**A**) while complementation of *trmJ* mutant strain (*trmJ*^{C}) restored the ribonucleoside levels (**B**). Data represent mean ± SD for three biological replicates, with asterisks denoting significant differences by Student's *t*-test ($P \leq 0.05$).

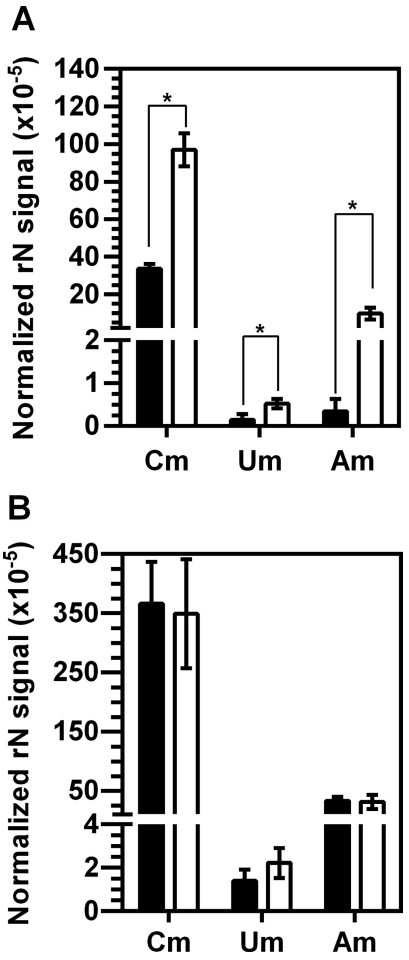

Figure 4. Purified PA14 TrmJ catalyzes Cm, Um and Am formation in total tRNA isolated from *P. aeruginosa trmJ* mutant. (**A**) Total tRNA extracted from the *trmJ* mutant strain was reacted with PA14 TrmJ and SAM (white bar) or left untreated (black bar), followed by LC–MS/MS quantification of Cm, Um and Am. (**B**) Total tRNA extracted from wild-type *P. aeruginosa* was reacted with PA14 TrmJ and SAM (white bar) or left untreated (black bar), followed by LC–MS/MS quantification of Cm, Um and Am. Data represent mean ± SD for three biological replicates for (**A**) and mean ± SD for two biological replicates for (**B**). Asterisks denote a significant difference by Student's *t*-test ($P \leq 0.05$).

gin molecules such that two tRNA molecules can in principle bind simultaneously at opposite faces of the TrmJ–NTD dimer (Figure 7). A view of the TrmJ–NTD dimer electrostatic surface reveals basic patches at the dimer surface. In this respect, the basic loop spanning residues 82-RDRRIPWL-90 is well positioned to bind the target tRNA substrate. This segment appears to be flexible both in the free I TrmJ–NTD and in the sinefungin-bound structures and probably requires tRNA to become ordered, as was indeed recently observed for a complex between the TrmD methyltransferase and tRNA (37).

Upon sinefungin binding, an outward opening movement towards the adjacent monomer occurs in loop 115-GREYAG-120 that acts as a lid to grant access to the inhibitor. The sinefungin molecule adopts a bent conformation within a pocket formed at the TrmJ–NTD dimer interface. Sinefungin appears to be primarily held via its adenine ring and sugar moieties, while its amino-acid tail is more mobile and extends towards the solvent. The catalytic residues Arg23 (from monomer A) and Ser 143 (monomer B) are both within hydrogen bonding distances of the sinefungin amino-group (which substitutes the methyl group in SAM) and make contact with two bound water molecules (Figure 8).

Molecular basis for TrmJ-dependent H_2O_2 sensitivity in *P. aeruginosa*

Having established that PA14_14690 codes for a tRNA:Cm32/Um32/Am32 methyltransferase that confers resistance to H_2O_2 in *P. aeruginosa*, we initiated studies to define the molecular basis for this behavior. We first assessed the role of catalase activity in the H_2O_2 sensitivity of the *trmJ* mutant. Catalase is one of the major enzymes involved in detoxification of H_2O_2, with PA14 possessing three genes (*katA*, *katB*, and *katE*) coding for catalases. Under unstressed conditions, catalase activity in the *trmJ* mutant strain (78 ± 3.2 unit/mg) was significantly lower than the wild-type and *trmJ*^{C} strains (95 ± 4.2 and 101 ± 6.9 unit/mg, respectively) (Figure 9A). This difference more than doubled when the cells were exposed to a roughly LD_{50} dose of H_2O_2, with catalase activity increasing 2.5-fold in wild-type cells compared to only 1.5-fold in the

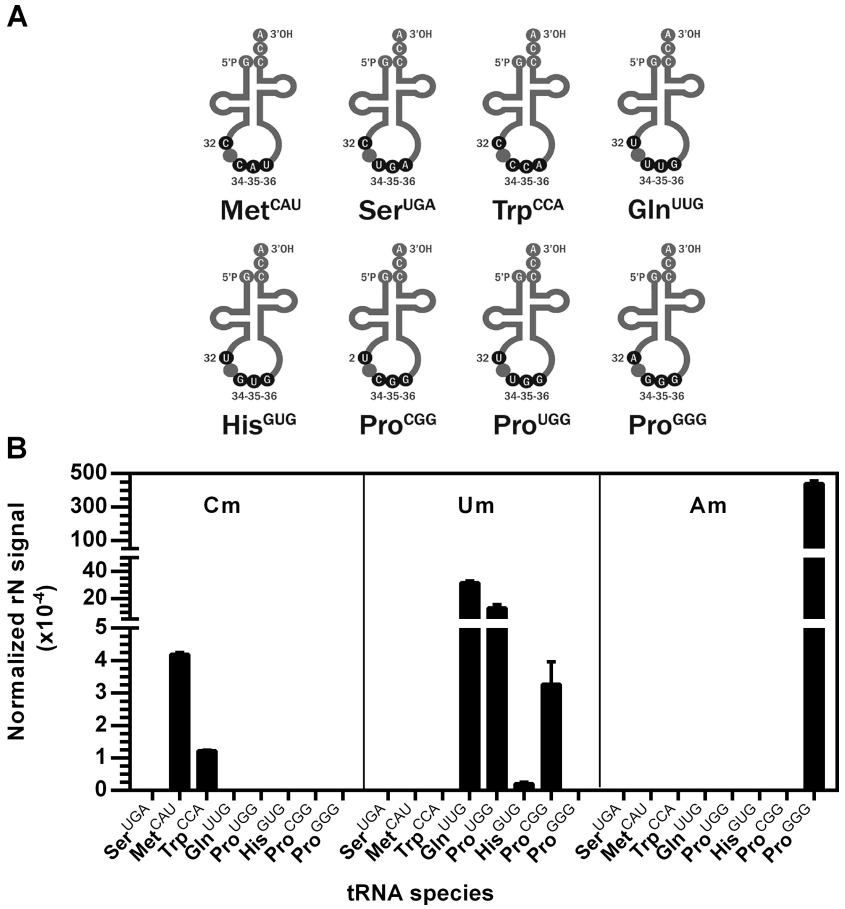

Figure 5. *In vitro* methylation of synthetic tRNAs by purified PA14 TrmJ. (**A**) The indicated tRNAs were prepared by *in vitro* transcription and used as substrates for *in vitro* methylation reactions with PA14 TrmJ and SAM. (**B**) Following LC–MS/MS analysis, signals for Cm, Um and Am were normalized to total signal for canonical A, C, G and U. Data represent mean ± SD for three biological replicates.

trmJ mutant strain (Figure 9A). TrmJ complementation restored the catalase activity to nearly wild-type levels (2.1-fold, $P < 0.05$) (Figure 9A).

These results suggest that TrmJ confers H_2O_2 resistance in part by upregulating the expression of catalase genes. To test this hypothesis at the transcriptional level, we quantified expression of *katA*, *katB*, and *katE* by semi-quantitative real-time PCR in total RNA isolated from wild-type, *trmJ* mutant, and *trmJ*^{C} strains exposed to 10 mM H_2O_2. In unexposed cells, the *katA*, *katB* and *katE* transcript levels were similar in all of the strains (Figure 9B–G). Upon exposure to 10 mM H_2O_2, however, *katB* and *katE* transcript levels increased more in the wild-type and *trmJ*^{C} strains than in the *trmJ* mutant (Figure 9C and D). We observed a similar pattern for *ankB* transcript levels (Figure 9E) as expected since *katB* and *ankB* are co-expressed on the same operon. Surprisingly, H_2O_2 caused higher levels of *katA* transcripts in *trmJ* mutant than in wild-type and *trmJ*^{C} strains (Figure 9B).

It is well recognized that OxyR is a key transcription regulator that modulates expression of antioxidant genes including *katB-ankB* and *katA* upon H_2O_2 stress in *P. aeruginosa* (16,38). We then investigated the expression level of *oxyR-recG* operon. The expression level of *oxyR-recG* was decreased in *trmJ* mutant strain after H_2O_2 exposure (Figure 9F,G). This is in good agreement with the expression pattern of *katB*. Considering these findings together, it suggests that *trmJ* is essential for a proper expression of *katB* during H_2O_2 stress through a modulation of *oxyR* expression.

DISCUSSION

Emerging evidence points to a variety of functions for tRNA other than as a simple adaptor molecule in protein synthesis (4,6–8). The potential for the functional diversity of tRNA is enhanced by dozens of post-transcriptional modifications of the canonical ribonucleotides, ranging from simple methylations as in 5-methylcytidine (m^5C) to hyper-modified bases as in 5-methoxycarbonylmethyluridine (mcm^5U). Here, we report that the gene for the tRNA methyltransferase *trmJ* in *P. aeruginosa* plays a role in the oxidative stress response, with its repertoire of position 32 anti-codon loop 2′-*O*-methylation products expanded from Um and Cm to include Am. This new function for TrmJ in oxidative stress response is consistent with similar roles for wobble m^5C in yeast tRNA (7,8) and the m^6A37 tRNA methyltransferase encoded by the *yfic* gene in *E. coli* (39).

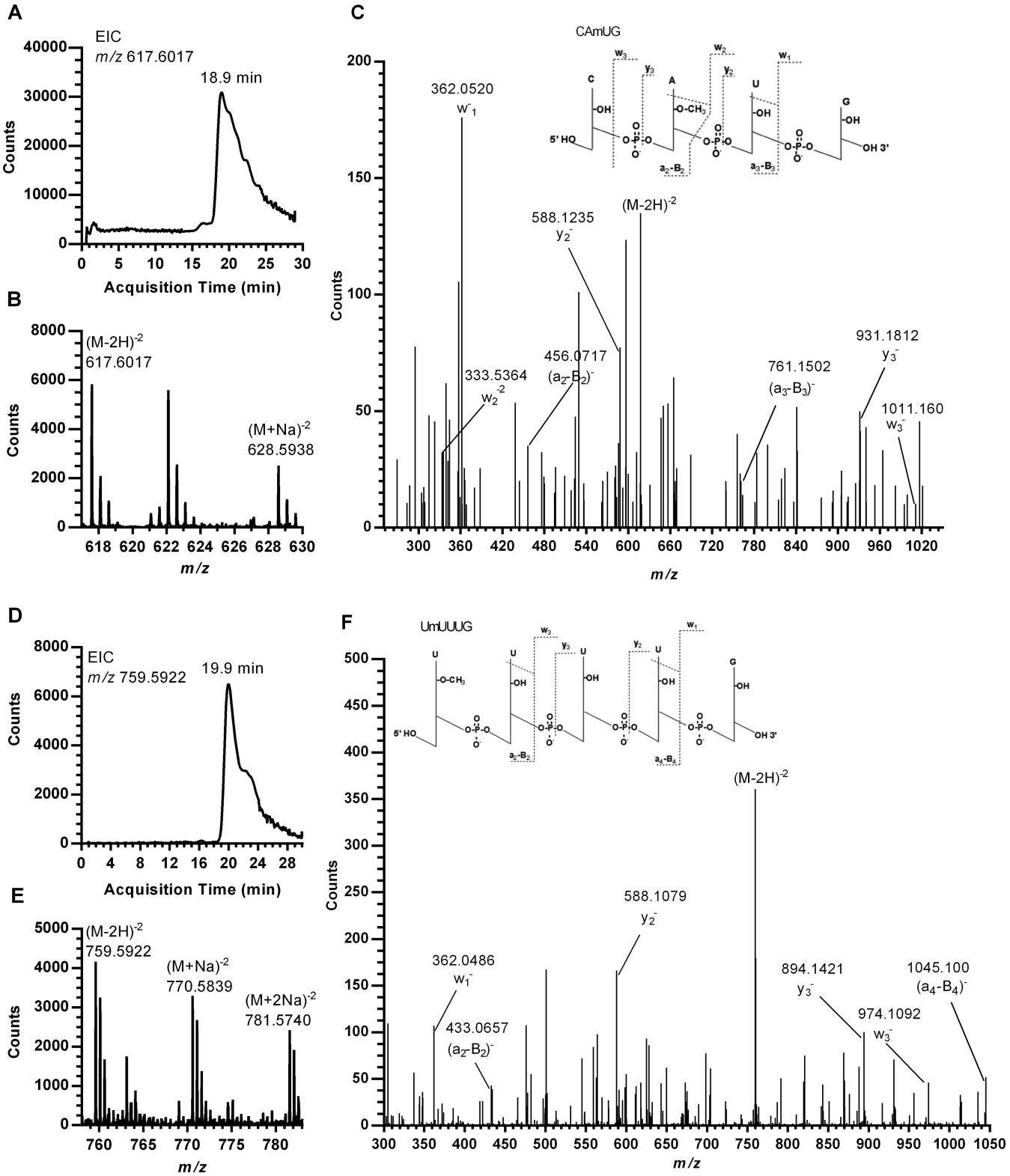

Figure 6. Mapping PA14 TrmJ methylation in tRNA by LC-QTOF analysis of RNase T1 digestion products. (**A**) Extracted ion chromatogram for *m/z* 617.6017 released from $tRNA^{Pro(GGG)}$ by RNase T1. (**B**) The mass spectrum for the $tRNA^{Pro(GGG)}$ oligo eluting at 18.9 min shows an $(M\text{-}2H)^{-2}$ ion with *m/z* 617.6017 and a sodium adduct at *m/z* 628.5938. (**C**) CID of *m/z* 617.6017 yields products consistent with CAmUG. (**D**) Extracted ion chromatogram for *m/z* 759.5922 released from $tRNA^{Gln(UUG)}$ by RNase T1. (**E**) The mass spectrum for the $tRNA^{Gln(UUG)}$ oligo eluting at 19.9 min shows an $(M\text{-}2H)^{-2}$ ion with *m/z* 759.5922 and sodium adducts at *m/z* 770.5839 and 781.5740. (**F**) CID spectrum of *m/z* 759.5922 yields products consistent with UmUUUG.

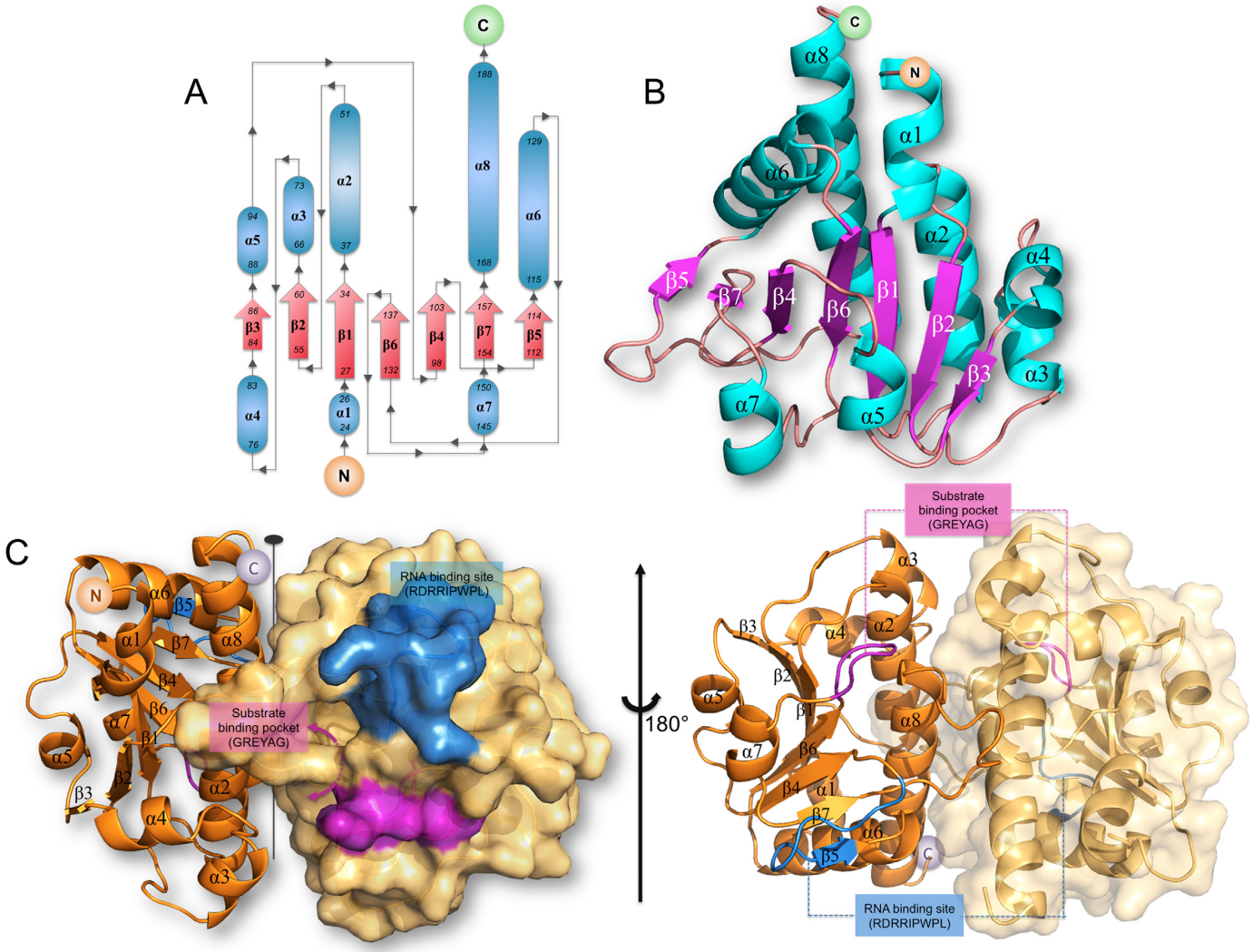

Figure 7. Overall structure of TrmJ–NTD from *P. aeruginosa.* (**A**) Topology of the SAM binding domain of TrmJ–NTD. The residue numbers and N- and C-termini of the polypeptide chain are indicated. (**B**) Structure of the TrmJ–NTD monomer using the same color code. (**C**) Left panel: Structure of the TrmJ–NTD homodimer. One monomer is depicted as 'ribbons' while a surface view is given for the other monomer. The SAM binding loop and the putative RNA binding residues are colored in purple and blue, respectively. The right panel shows a view rotated by 180° along a vertical axis emphasizing the tight dimer interface contributed by two long helices and projecting loops.

PA14 TrmJ shares most of the important characteristics found in other bacterial homologs, including a TrmJ-specific motif (a consensus 'TXARXR' sequence) important for binding to SAM/SAH and tRNA, a conserved amino acid important for catalytic activity, and conserved amino acids at the C-terminus (Figure 2) (33). This conservation is reinforced in the structural analysis shown in Figures 7 and 8. Arg23 and Ser43 are evolutionary conserved and correspond to Arg23 and Ser142 in TrmJ from *E. coli*. However, the TrmJ–NTD catalytic site from *P. aeruginosa* displays an interesting difference with *E. coli* TrmJ: the residue structurally equivalent to Tyr140 of *E. coli* TrmJ, that was proposed to play a catalytic role, is substituted by Phe141 in the *P. aeruginosa* enzyme. The only other possible residue in the catalytic site with a hydroxyl group is Tyr118, which does not establish an H-bond with Arg21.

The substrate specificity of PA14 TrmJ also shows similarities to and notable differences from other TrmJ homologs. We found that PA14 TrmJ catalyzes the formation not only of Cm and Um at position 32 in tRNA, but also Am *in vivo* and *in vitro* (Figures 3–6). While the data in Figure 5B represent population levels of Cm, Um and Am in tRNA hydrolysates, the fact that these TrmJ products were only observed in the tRNAs that possessed the specific respective C32, U32, and A32 substrates is consistent with the established specificity of TrmJ for position 32. Though possible, it is unlikely that the Am observed in $tRNA^{Pro(GGG)}$ occurred at positions other than 32. In the archaean *Sulfolobus acidocaldarius,* it has been shown that TrmJ performs ribose methylation at only C32 both *in vivo* and *in vitro*. *E. coli* possesses two activities catalyzing both Cm and Um *in vitro* and *in vivo*, TrmJ and TrmL, with TrmJ methylating position 32 (34,40) and TrmL methylating the wobble position 34 in leucine tRNA isoacceptors (41). Such an enzymatic redundancy may explain the observation of high background levels of Cm in the PA14 *trmJ*

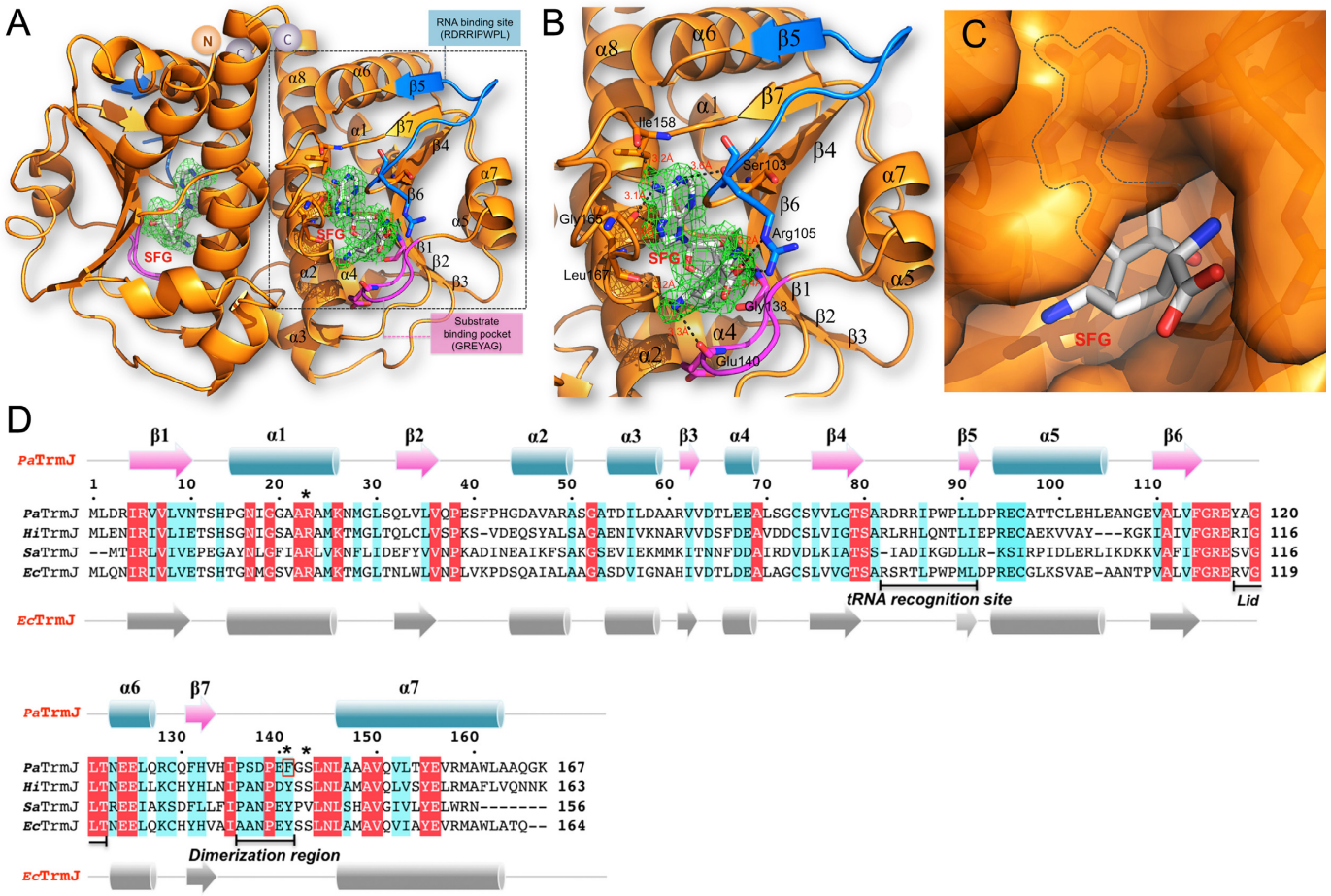

Figure 8. Sinefungin (SFG) binding by TrmJ–NTD from *P. aeruginosa.* (**A**) Two sinefungin molecules (sticks) are bound to the TrmJ–NTD homodimer displayed as an orange ribbons. An electron density map with Fourier coefficients mFo-DFc and phases where the SFG molecules were omitted from the calculation is displayed in green at a level of 3 Å. (**B** and **C**) Magnified views of the cofactor-binding site highlighting residues interacting with SFG. Hydrogen bonds are displayed as dashed lines. (**C**) TrmJ–NTD is shown as a molecular surface and SFG is represented as sticks with the base deeply buried in the pocket whilst the amino-acid tail projects towards the solvent. (**D**) Structure based sequence alignment of the NTD domains of TrmJ from *Pseudomonas aeruginosa* (PA14 TrmJ, this work), *Haemophilus influenzae* TrmJ (HiTrmJ), *Sulfolobus acidocaldarius* (SaTrmJ) and *E. coli* (EcTrmJ) (34). Strictly conserved residues are highlighted in red and conserved residues in cyan. Deletions are indicated by dashes. The secondary structure of PA14 TrmJ is shown above the sequence.

mutant strain (Figure 3). The observation of Am32 and Gm32 in tRNA with *E. coli* TrmJ was made with a single tRNA species that varied the identity of the ribonucleoside at position 32 and thus does not represent a biologically-relevant activity (34). In terms of substrates, 7 tRNA substrates were identified for PA14 TrmJ *in vitro*: $tRNA^{Met(CAU)}$ and $tRNA^{Trp(CCA)}$ for C32; $tRNA^{Gln(UUG)}$, $tRNA^{Pro(UGG)}$, $tRNA^{Pro(CGG)}$ and $tRNA^{His(GUG)}$ for U32; and A32 in $tRNA^{Pro(GGG)}$ (Figure 5). Similar *in vitro* studies with *E. coli* TrmJ revealed 4 substrates overlapping with PA14 ($tRNA^{Met(CAU)}$, $tRNA^{Trp(CCA)}$ and $tRNA^{Gln(UUG)}$) and two different substrates: $tRNA^{Gln(CUG)}$ and $tRNA^{Ser(UGA)}$ (33).

One new function of TrmJ activity arises from our observation that hypomethylation of 2′-*O*-ribose moiety of C32, U32, and A32 of tRNA in the PA14 *trmJ* mutant strain rendered the cells hypersensitive to the oxidative stress of H_2O_2 exposure. This parallels the resistance to oxidative stress conferred by m^6A37 in tRNA in *E. coli* (39). One mechanism underlying the H_2O_2 sensitivity of the PA14 *trmJ* mutant strain involves reduced catalase activity (Figure 9A). It is not clear which of the 3 catalase genes in PA14 have reduced activity, since 2 genes (*katB* and *katE*) showed reduced mRNA levels in the *trmJ* mutant strain exposed to H_2O_2, while the major catalase, KatA, had higher mRNA levels (Figure 9C and D). Although KatE is generally regarded as stationary phase catalase, it has also been shown to protect bacteria against oxidative stress during logarithmic phase of growth (42–44). The expression of *katB* is known to be under the regulation of OxyR, an oxidation-sensing transcription regulator (16,45). The lower level of *katB* in the *P. aeruginosa trmJ* mutant during H_2O_2 stress may thus result from lower expression of OxyR.

So what are the mechanistic links between a defect in 2′-*O*-methylation of C, U and A at position 32 of the tRNA anticodon loop and H_2O_2 resistance in PA14? Modifications of tRNA anticodon loop have been demonstrated to play a role in stabilizing local structure and enhancing accurate codon recognition (46). For example, lack of 2-

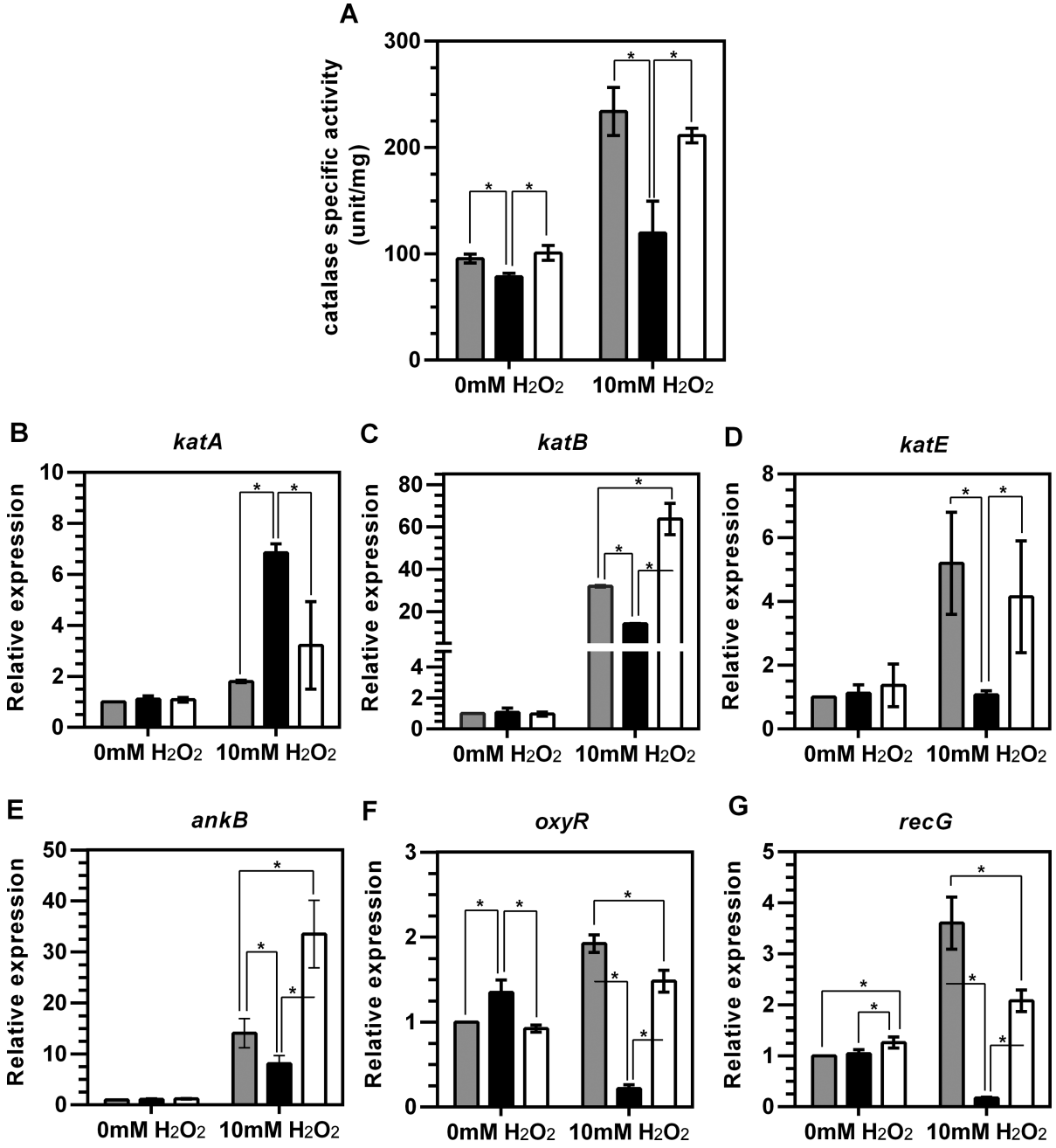

Figure 9. Loss of *trmJ* causes a decreased catalase activity and alters expression of oxidative stress responsive genes. (**A**) Catalase activity assay in PA14 wild-type strain (grey bar), *trmJ* mutant strain (black bar), and the *trmJ* complementation strain or $trmJ^C$ (white bar). (**B-G**) Quantitative real time PCR analysis of oxidative stress responsive genes**.** Bacterial cultures were grown to exponential phase ($OD_{600} \approx 0.4$) and were then either treated or untreated with 10 mM H_2O_2 for 25 min. Expression of *katA* (**B**), *katB* (**C**), *katE* (**D**), *ankB* (**E**), *oxyR* (**F**), and *recG* (**G**) in *trmJ* mutant strain (black bar) and $trmJ^C$ (white bar) was reported as fold-change in expression relative to the level of that gene in the PA14 wild-type strain (grey bar) without H_2O_2 treatment. The data represent mean ± SD for three biological replicates. Asterisks denote the values with significant difference by Student's *t*-test ($P \leq 0.05$).

thiocytidine (s^2C) at position 32 of $tRNA^{Arg}$ can destabilize the anticodon loop (3), reduce the A-site selection rate for $tRNA^{Arg(mnm5UCU)}$ at the AGG codon, and increase the frequency of frameshifting (47). Comparing 2-thiolation and 2′-*O*-methylation of ribonucleotides, both stabilize the C3′-endoform of pyrimidine nucleotides (48,49) and enhance base stacking (50). So, one possible role of 2′-*O*-methylation at position 32 of tRNA ribonucleotides could be to improve anticodon loop stability and anticodon base-paring properties of tRNA. Thus, it is possible that the lack of Cm32, Um32, and Am32 in tRNA could reduce the paring properties of tRNA and thus cause inefficient translation or misreading of mRNAs for proteins crucial oxidative stress response in *P. aeruginosa*. Evidence in yeast has shown that a defect in position 32 2′-*O*-methylation caused by loss of Trm7 impairs growth and translation effi-

ciency and fidelity (51,52). Interestingly, loss of TrmJ activity did not affect PA14 susceptibility to the oxidative stressors paraquat and t-butyl hydroperoxide, which indicates a specificity of TrmJ-dependent tRNA modifications for affecting an H_2O_2 survival phenotype in PA14. Similarly, Chan et al. observed that Trm4 protected yeast against H_2O_2 toxicity, while Trm9 and Trm140 protected against exposure to alkylating agents (53). There is a strong parallel here in terms of fine-tuning the stress response to specific agents. Yeast Trm140 inserts m^3C at position 32 in three tRNAs ($tRNA^{Thr(IGU)}$, $tRNA^{Ser(UGA)}$, $tRNA^{Ser(CGA)}$) and selectively protects against S_N1-type alkylating agents such as methyl- and ethyl-methanesulfonate (MMS and EMS, respectively) but not S_N2 alkylators (53). It awaits further study to determine if the oxidative stress sensitivity in PA14 is the result of reduced translation of transcripts with codon biases that match TrmJ-dependent tRNAs, as occurs with Trm4, Trm9 and Trm140 in yeast (7,53). Such a mechanism could explain how loss of TrmJ leads to reduced transcription of *oxyR* and its regulon, if the transcriptional regulators of *oxyR* or other up-stream stress response genes are enriched in TrmJ-dependent codons.

In summary, we present results demonstrating that PA14 TrmJ is a tRNA methyltransferase that catalyzes formation of Cm, Um and Am at position 32 and that TrmJ protects PA14 against H_2O_2-induced toxicity. The results point to a mechanism linking tRNA modifications to stress response phenotypes in bacteria.

SUPPLEMENTARY DATA

Supplementary Data are available at NAR Online.

ACKNOWLEDGEMENTS

The authors thank Mr. Ee Pin Koon for technical assistance with synthesis and purification of tRNA, Ms. Maggie Cai for technical assistance with QQQ operation, Ms. Thanyaporn Srimahaeak for handling of bacterial strains, Dr. Amnart Khongmanee and Mr. Bhawat Wongkhamprai for technical assistance with QTOF analysis, and NISB for sharing the Swiss Light Source and Taiwan Light Source synchrotron beamtime.

FUNDING

National Research Foundation of Singapore through its Singapore-MIT Alliance for Research and Technology; US National Science Foundation [CHE-1308839]; Chulabhorn Graduate Institute; Chulabhorn Research Institute; Mahidol University; Agilent Technologies. Funding for open access charge: Chulabhorn Research Institute and Chulabhorn Graduate Institute.
Conflict of interest statement. None declared.

REFERENCES

1. El Yacoubi,B., Bailly,M. and de Crecy-Lagard,V. (2012) Biosynthesis and function of posttranscriptional modifications of transfer RNAs. *Annu. Rev. Genet.*, **46**, 69–95.
2. Bjork,G.R., Wikstrom,P.M. and Bystrom,A.S. (1989) Prevention of translational frameshifting by the modified nucleoside 1-methylguanosine. *Science*, **244**, 986–989.
3. Cantara,W.A., Bilbille,Y., Kim,J., Kaiser,R., Leszczynska,G., Malkiewicz,A. and Agris,P.F. (2012) Modifications modulate anticodon loop dynamics and codon recognition of *E. coli* $tRNA^{Arg1,2}$. *J. Mol. Biol.*, **416**, 579–597.
4. Patil,A., Chan,C.T., Dyavaiah,M., Rooney,J.P., Dedon,P.C. and Begley,T.J. (2012) Translational infidelity-induced protein stress results from a deficiency in Trm9-catalyzed tRNA modifications. *RNA Biol.*, **9**, 990–1001.
5. Urbonavicius,J., Qian,Q., Durand,J.M., Hagervall,T.G. and Bjork,G.R. (2001) Improvement of reading frame maintenance is a common function for several tRNA modifications. *EMBO J.*, **20**, 4863–4873.
6. Chan,C.T., Dyavaiah,M., DeMott,M.S., Taghizadeh,K., Dedon,P.C. and Begley,T.J. (2010) A quantitative systems approach reveals dynamic control of tRNA modifications during cellular stress. *PLoS Genet.*, **6**, e1001247.
7. Chan,C.T., Pang,Y.L., Deng,W., Babu,I.R., Dyavaiah,M., Begley,T.J. and Dedon,P.C. (2012) Reprogramming of tRNA modifications controls the oxidative stress response by codon-biased translation of proteins. *Nat. Commun.*, **3**, 937.
8. Begley,U., Dyavaiah,M., Patil,A., Rooney,J.P., DiRenzo,D., Young,C.M., Conklin,D.S., Zitomer,R.S. and Begley,T.J. (2007) Trm9-catalyzed tRNA modifications link translation to the DNA damage response. *Mol. Cell*, **28**, 860–870.
9. Arancibia,F., Bauer,T.T., Ewig,S., Mensa,J., Gonzalez,J., Niederman,M.S. and Torres,A. (2002) Community-acquired pneumonia due to gram-negative bacteria and *Pseudomonas aeruginosa*: incidence, risk, and prognosis. *Arch. Intern. Med.*, **162**, 1849–1858.
10. Solomon,S.L. and Oliver,K.B. (2014) Antibiotic resistance threats in the United States: stepping back from the brink. *Am. Family Phys.*, **89**, 938.
11. Gellatly,S.L. and Hancock,R.E. (2013) *Pseudomonas aeruginosa*: new insights into pathogenesis and host defenses. *Pathog. Dis.*, **67**, 159–173.
12. Reinhart,A.A., Powell,D.A., Nguyen,A.T., O'Neill,M., Djapgne,L., Wilks,A., Ernst,R.K. and Oglesby-Sherrouse,A.G. (2015) The *prrF*-encoded small regulatory RNAs are required for iron homeostasis and virulence of *Pseudomonas aeruginosa*. *Infect. Immun.*, **83**, 863–875.
13. Wei,Q., Minh,P.N., Dotsch,A., Hildebrand,F., Panmanee,W., Elfarash,A., Schulz,S., Plaisance,S., Charlier,D., Hassett,D. *et al.* (2012) Global regulation of gene expression by OxyR in an important human opportunistic pathogen. *Nucleic Acids Res.*, **40**, 4320–4333.
14. Atichartpongkul,S., Fuangthong,M., Vattanaviboon,P. and Mongkolsuk,S. (2010) Analyses of the regulatory mechanism and physiological roles of *Pseudomonas aeruginosa* OhrR, a transcription regulator and a sensor of organic hydroperoxides. *J. Bacteriol.*, **192**, 2093–2101.
15. Lan,L., Murray,T.S., Kazmierczak,B.I. and He,C. (2010) *Pseudomonas aeruginosa* OspR is an oxidative stress sensing regulator that affects pigment production, antibiotic resistance and dissemination during infection. *Mol. Microbiol.*, **75**, 76–91.
16. Ochsner,U.A., Vasil,M.L., Alsabbagh,E., Parvatiyar,K. and Hassett,D.J. (2000) Role of the *Pseudomonas aeruginosa oxyR-recG* operon in oxidative stress defense and DNA repair: OxyR-dependent regulation of *katB-ankB*, *ahpB*, and *ahpC-ahpF*. *J. Bacteriol.*, **182**, 4533–4544.
17. Palma,M., DeLuca,D., Worgall,S. and Quadri,L.E.N. (2004) Transcriptome analysis of the response of *Pseudomonas aeruginosa* to hydrogen peroxide. *J. Bacteriol.*, **186**, 248–252.
18. Alexeyev,M.F. (1999) The pKNOCK series of broad-host-range mobilizable suicide vectors for gene knockout and targeted DNA insertion into the chromosome of gram-negative bacteria. *Biotechniques*, **26**, 824–826.
19. Geng,X. and Oliver,G. (2010) Elucidating the molecular characteristics of organogenesis in human embryos. *Genome Biol.*, **11**, 130.
20. Grant,S.G., Jessee,J., Bloom,F.R. and Hanahan,D. (1990) Differential plasmid rescue from transgenic mouse DNAs into *Escherichia coli* methylation-restriction mutants. *Proc. Natl. Acad. Sci. U.S.A.*, **87**, 4645–4649.
21. Kovach,M.E., Elzer,P.H., Hill,D.S., Robertson,G.T., Farris,M.A., Roop,R.M. 2nd and Peterson,K.M. (1995) Four new derivatives of

the broad-host-range cloning vector pBBR1MCS, carrying different antibiotic-resistance cassettes. *Gene*, **166**, 175–176.
22. Lee,D.G., Urbach,J.M., Wu,G., Liberati,N.T., Feinbaum,R.L., Miyata,S., Diggins,L.T., He,J., Saucier,M., Deziel,E. *et al.* (2006) Genomic analysis reveals that *Pseudomonas aeruginosa* virulence is combinatorial. *Genome Biol.*, **7**, R90.
23. Metcalf,W.W., Jiang,W., Daniels,L.L., Kim,S.K., Haldimann,A. and Wanner,B.L. (1996) Conditionally replicative and conjugative plasmids carrying *lacZ* alpha for cloning, mutagenesis, and allele replacement in bacteria. *Plasmid*, **35**, 1–13.
24. Chan,C.T., Chionh,Y.H., Ho,C.H., Lim,K.S., Babu,I.R., Ang,E., Wenwei,L., Alonso,S. and Dedon,P.C. (2011) Identification of N6,N6-dimethyladenosine in transfer RNA from *Mycobacterium bovis* Bacille Calmette-Guerin. *Molecules*, **16**, 5168–5181.
25. Su,D., Chan,C.T., Gu,C., Lim,K.S., Chionh,Y.H., McBee,M.E., Russell,B.S., Babu,I.R., Begley,T.J. and Dedon,P.C. (2014) Quantitative analysis of ribonucleoside modifications in tRNA by HPLC-coupled mass spectrometry. *Nat. Protoc.*, **9**, 828–841.
26. Rozenski,J. and McCloskey,J.A. (2002) SOS: a simple interactive program for ab initio oligonucleotide sequencing by mass spectrometry. *J. Am. Soc. Mass Spectrom.*, **13**, 200–203.
27. Livak,K.J. and Schmittgen,T.D. (2001) Analysis of relative gene expression data using real-time quantitative PCR and the $2^{-\Delta\Delta C_T}$ method. *Methods*, **25**, 402–408.
28. Kabsch,W. (2010) Integration, scaling, space-group assignment and post-refinement. *Acta Crystallogr. D Biol. Crystallogr.*, **66**, 133–144.
29. Collaborative Computational Project, N. (1994) The CCP4 suite: programs for protein crystallography. *Acta Crystallogr. D Biol. Crystallogr.*, **50**, 760–763.
30. Emsley,P. and Cowtan,K. (2004) Coot: model-building tools for molecular graphics. *Acta Crystallogr. D Biol. Crystallogr.*, **60**, 2126–2132.
31. Smart,O.S., Womack,T.O., Flensburg,C., Keller,P., Paciorek,W., Sharff,A., Vonrhein,C. and Bricogne,G. (2012) Exploiting structure similarity in refinement: automated NCS and target-structure restraints in BUSTER. *Acta Crystallogr. D Biol. Crystallogr.*, **68**, 368–380.
32. Robert,X. and Gouet,P. (2014) Deciphering key features in protein structures with the new ENDscript server. *Nucleic Acids Res.*, **42**, W320–W324.
33. Liu,R.J., Long,T., Zhou,M., Zhou,X.L. and Wang,E.D. (2015) tRNA recognition by a bacterial tRNA Xm32 modification enzyme from the SPOUT methyltransferase superfamily. *Nucleic Acids Res.*, **43**, 7489–7503.
34. Somme,J., Van Laer,B., Roovers,M., Steyaert,J., Versees,W. and Droogmans,L. (2014) Characterization of two homologous 2′-*O*-methyltransferases showing different specificities for their tRNA substrates. *RNA*, **20**, 1257–1271.
35. Kurowski,M.A., Sasin,J.M., Feder,M., Debski,J. and Bujnicki,J.M. (2003) Characterization of the cofactor-binding site in the SPOUT-fold methyltransferases by computational docking of S-adenosylmethionine to three crystal structures. *BMC Bioinformatics*, **4**, 9.
36. Michel,G., Sauve,V., Larocque,R., Li,Y., Matte,A. and Cygler,M. (2002) The structure of the RlmB 23S rRNA methyltransferase reveals a new methyltransferase fold with a unique knot. *Structure*, **10**, 1303–1315.
37. Ito,T., Masuda,I., Yoshida,K., Goto-Ito,S., Sekine,S., Suh,S.W., Hou,Y.M. and Yokoyama,S. (2015) Structural basis for methyl-donor-dependent and sequence-specific binding to tRNA substrates by knotted methyltransferase TrmD. *Proc. Natl. Acad. Sci. U.S.A.*, **112**, E4197–E4205.
38. Heo,Y.J., Chung,I.Y., Cho,W.J., Lee,B.Y., Kim,J.H., Choi,K.H., Lee,J.W., Hassett,D.J. and Cho,Y.H. (2010) The major catalase gene (*katA*) of *Pseudomonas aeruginosa* PA14 is under both positive and negative control of the global transactivator OxyR in response to hydrogen peroxide. *J. Bacteriol.*, **192**, 381–390.
39. Golovina,A.Y., Sergiev,P.V., Golovin,A.V., Serebryakova,M.V., Demina,I., Govorun,V.M. and Dontsova,O.A. (2009) The *yfiC* gene of *E. coli* encodes an adenine-N6 methyltransferase that specifically modifies A37 of $tRNA_1^{Val}(cmo^5UAC)$. *RNA*, **15**, 1134–1141.
40. Purta,E., van Vliet,F., Tkaczuk,K.L., Dunin-Horkawicz,S., Mori,H., Droogmans,L. and Bujnicki,J.M. (2006) The *yfhQ* gene of *Escherichia coli* encodes a tRNA:Cm32/Um32 methyltransferase. *BMC Mol. Biol.*, **7**, 23.
41. Benitez-Paez,A., Villarroya,M., Douthwaite,S., Gabaldon,T. and Armengod,M.E. (2010) YibK is the 2'-*O*-methyltransferase TrmL that modifies the wobble nucleotide in *Escherichia coli* $tRNA^{Leu}$ isoacceptors. *RNA*, **16**, 2131–2143.
42. Ivanova,A.B., Glinsky,G.V. and Eisenstark,A. (1997) Role of *rpoS* regulon in resistance to oxidative stress and near-UV radiation in delta *oxyR* suppressor mutants of *Escherichia coli*. *Free Radic. Biol. Med.*, **23**, 627–636.
43. Miller,C.D., Kim,Y.C. and Anderson,A.J. (1997) Cloning and mutational analysis of the gene for the stationary-phase inducible catalase (*catC*) from *Pseudomonas putida*. *J. Bacteriol.*, **179**, 5241–5245.
44. Vattanaviboon,P. and Mongkolsuk,S. (2000) Expression analysis and characterization of the mutant of a growth-phase- and starvation-regulated monofunctional catalase gene from *Xanthomonas campestris* pv phaseoli. *Gene*, **241**, 259–265.
45. Panmanee,W. and Hassett,D.J. (2009) Differential roles of OxyR-controlled antioxidant enzymes alkyl hydroperoxide reductase (AhpCF) and catalase (KatB) in the protection of *Pseudomonas aeruginosa* against hydrogen peroxide in biofilm vs. planktonic culture. *FEMS Microbiol. Lett.*, **295**, 238–244.
46. Agris,P.F. (2008) Bringing order to translation: the contributions of transfer RNA anticodon-domain modifications. *EMBO Rep.*, **9**, 629–635.
47. Jager,G., Leipuviene,R., Pollard,M.G., Qian,Q. and Bjork,G.R. (2004) The conserved Cys-X1-X2-Cys motif present in the TtcA protein is required for the thiolation of cytidine in position 32 of tRNA from *Salmonella enterica* serovar Typhimurium. *J. Bacteriol.*, **186**, 750–757.
48. Kawai,G., Yamamoto,Y., Kamimura,T., Masegi,T., Sekine,M., Hata,T., Iimori,T., Watanabe,T., Miyazawa,T. and Yokoyama,S. (1992) Conformational rigidity of specific pyrimidine residues in tRNA arises from posttranscriptional modifications that enhance steric interaction between the base and the 2'-hydroxyl group. *Biochemistry*, **31**, 1040–1046.
49. Yamamoto,Y., Yokoyama,S., Miyazawa,T., Watanabe,K. and Higuchi,S. (1983) NMR analyses on the molecular mechanism of the conformational rigidity of 2-thioribothymidine, a modified nucleoside in extreme thermophile tRNAs. *FEBS Lett.*, **157**, 95–99.
50. Drake,A.F., Mason,S.F. and Trim,A.R. (1974) Optical studies of the base-stacking properties of 2'-*O*-methylated dinucleoside monophosphates. *J. Mol. Biol.*, **86**, 727–739.
51. Guy,M.P., Podyma,B.M., Preston,M.A., Shaheen,H.H., Krivos,K.L., Limbach,P.A., Hopper,A.K. and Phizicky,E.M. (2012) Yeast Trm7 interacts with distinct proteins for critical modifications of the $tRNA^{Phe}$ anticodon loop. *RNA*, **18**, 1921–1933.
52. Pintard,L., Lecointe,F., Bujnicki,J.M., Bonnerot,C., Grosjean,H. and Lapeyre,B. (2002) Trm7p catalyses the formation of two 2'-*O*-methylriboses in yeast tRNA anticodon loop. *EMBO J.*, **21**, 1811–1820.
53. Chan,C.T., Deng,W., Li,F., DeMott,M.S., Babu,I.R., Begley,T.J. and Dedon,P.C. (2015) Highly predictive reprogramming of tRNA modifications is linked to selective expression of codon-biased genes. *Chem. Res. Toxicol.*, **28**, 978–988.